ARTICLE

Nanoimprint-Induced Molecular Orientation in Semiconducting Polymer Nanostructures

Htay Hlaing,[†,‡] Xinhui Lu,[†] Tommy Hofmann,[†] Kevin G. Yager,[§] Charles T. Black,[§] and Benjamin M. Ocko[†,*]

[†]Condensed Matter Physics and Materials Science Department, Brookhaven National Laboratory, Upton, New York 11973, United States, [‡]Department of Physics and Astronomy, State University of New York, Stony Brook, New York 11794, United States, and [§]Center for Functional Nanomaterials, Brookhaven National Laboratory, Upton, New York 11973, United States

ABSTRACT The morphology and orientation of thin films of the polymer poly-3(hexylthiophene)— important parameters influencing electronic and photovoltaic device performance—have been significantly altered through nanoimprinting with 100 nm spaced grooves. Grazing-incidence small-angle X-ray scattering studies demonstrate the excellent fidelity of the pattern transfer, while wide-angle scattering convincingly shows an imprinting-induced $\pi-\pi$ reorientation and polymer backbone alignment along the imprinted grooves. Surprisingly, temperature-dependent scattering measurements indicate that the imprinted induced orientation and alignment remain intact even at temperatures where the imprinted topographical features nearly vanish.

KEYWORDS: nanoimprint · organic semiconductor · nanoscale morphology · polymer chain orientation · GISAXS · GIWAXS

Nanoimprinting provides a route for controlling the morphology of functional polymer nanostructures[1−5] in addition to its originally intended application as a high-resolution lithographic technique.[6−8] Thin organic films, including light-emitting conjugated polymers,[1] block copolymers,[2] piezoelectric polymers,[3] and semicrystalline polymers,[4,5] have been directly patterned using nanoimprinting to obtain desired morphological features. More recent studies have shown that nanoimprinting can control the molecular chain configurations of liquid-crystalline polymers such as poly(9,9-dioctylfluorene-*co*-benzothiadiazole).[9] For thermoplastic fluoropolymers (*e.g.*, polyvinylidene fluoride), this method also induces preferential polymer chain alignment.[3,10]

In this work, we investigate nanoimprinting as a means to control both the morphology and molecular chain orientation of thin-film conjugated polymers. These properties are inherently difficult to control in conjugated polymers such as poly-3(hexyl thiophene) (P3HT) and have a profound effect on the electrical and optical performance. For example, a thin film's molecular chain orientation depends on processing conditions such as the casting solvent, method of deposition (*e.g.*, spin-coating, blade-coating), and substrate surface treatment.[11−14] P3HT films cast from slowly evaporated solvents exhibit polymer chains oriented with their $\pi-\pi$ stacking direction in the plane of the substrate and their corresponding side-chain-induced lamellar structure stacked substrate-normal (Figure 1a, edge-on orientation), with the degree of crystallinity, domain size, and orientation dependent on the polymer's molecular weight and regioregularity.[14−16] In contrast, P3HT films cast from fast-evaporating solvents (*e.g.*, chloroform) have some degree of $\pi-\pi$ stacking along the substrate-normal with their lamellar structure arranged substrate-parallel (Figure 1a, face-on orientation) but with the polymer backbone randomly oriented in the surface plane.[11] The thermal stability of the face-on orientation has not been studied in detail, and it is possible that some of these structures are kinetically trapped, rather than thermodynamically stable orientations. Controlling the P3HT polymer chain orientation is important because of its strongly anisotropic electrical conductivity, where the charge carrier mobility in the plane of $\pi-\pi$ stacking and the conjugated backbone can be several orders of magnitude higher than that in the lamellar stacking direction, where carriers must traverse the insulating P3HT alkyl chains.[13,17] While an edge-on chain orientation is desirable for devices having in-plane charge transport (*e.g.*, transistors), a face-on orientation benefits architectures with charge transport normal to the substrate plane, such as solar cells or light-emitting diodes.

Here, we show that nanoimprint methods can transfer topographical features from the imprint master to a P3HT film with high fidelity, and further that the imprint process reorients some of the polymer material from

* Address correspondence to ocko@bnl.gov.

Received for review July 6, 2011 and accepted August 12, 2011.

Published online August 12, 2011
10.1021/nn202515z

© 2011 American Chemical Society

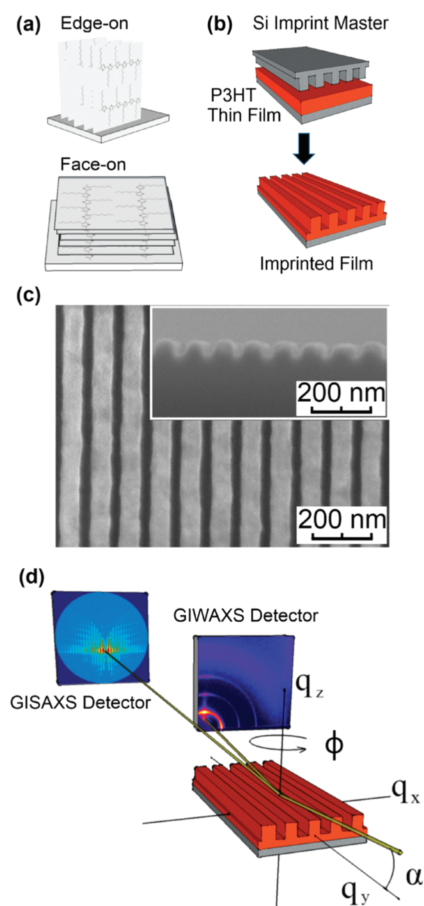

Figure 1. Schematics of (a) edge-on and face-on orientation of P3HT domains and (b) the nanoimprint process. (c) SEM image of the imprinted P3HT gratings with a 100 nm period (inset: grating cross-sectional view). (d) Geometry of GISAXS/GIWAXS measurements.

edge-on to face-on. The P3HT backbones are well-aligned along the grating direction, in contrast to a previously published study which reported that the P3HT backbones are oriented vertically in the nanogratings with π-stacking along the grating direction.[18] The utilization of a synchrotron X-ray source, coupled with area detectors and precise control of the sample angles, has enabled unambiguous mapping of the polymer chain orientation.

RESULTS AND DISCUSSION

The imprinted film's nanostructure and its molecular chain configurations were investigated *in situ* using grazing-incidence small- and wide-angle X-ray scattering (GISAXS and GIWAXS). From the GISAXS pattern analysis, we extracted the periodicity, height, side-wall angle, and the relative roughness of the top and bottom surfaces of the P3HT nanostructure. Detailed characterizations of the P3HT structure, including their molecular orientations within the nanostructure, were obtained from the GIWAXS measurements. In order to obtain insight into the thermal stability of the nanoimprinted P3HT films, essential information for the fabrication process, and to assess the impact of heating effects for organic photovoltaic applications, temperature-dependent studies were also carried out on the nanoimprinted P3HT films.

The imprinting process involved applying a pressure of 3.4 MPa between the master and the coated polymer substrate stack at 150 °C for 5 min (schematic in Figure 1b); the stack was then quenched to room temperature before releasing the applied pressure. Top-down and cross-sectional SEM images confirm a uniformly imprinted P3HT film (Figure 1c). The GISAXS and GIWAXS experiments were performed at the X9 undulator beamline at the NSLS (Brookhaven National Laboratory) where the 14.0 keV photons (λ = 0.0886 nm) are focused to a spot 80 μm high and 200 μm wide at the sample position. Figure 1d shows the experimental geometry of the X-ray measurements (described in the Methods and Materials section).

We define the scattering vector, $\mathbf{q} = (q_x, q_y, q_z)$ with q_y aligned along the groove direction, q_x orthogonal to q_y in the film plane, and q_z pointing along the surface normal. Since a CCD image for a sample with a fixed azimuthal angle ϕ has both q_x and q_y components, it is convenient to define the surface radial component $q_r = (q_x^2 + q_y^2)^{1/2}$, whose value is independent of ϕ, the angle between the direction of the grooves, and the incident X-rays. To acquire the GISAXS images in Figure 2a,b, the sample was rotated at a constant speed over a limited ϕ range.[19] Note that the maximum q_z increases with the ϕ range[20] (±1 or ±3°) and that at the smallest q_r the q_z range is restricted (see Figure 2a,b).

The GISAXS patterns from the silicon imprint master and imprinted P3HT film are sensitive to morphological features and exhibit a high degree of similarity (Figure 2a, b). Both patterns exhibit scattering features along q_z at evenly spaced values of q_r, known as Bragg rods (BRs). The BR's sinusoidal-like intensity modulation is characteristic of a relative scattering phase factor equal to $H \times q_z$, where H is the height difference between the top and bottom of the pattern. According to Babinet's Principle,[21] diffraction from a pattern and its complement are equal apart from an intensity scale factor, and thus the similar scattering images from the master and the imprinted P3HT provide a measure of the high fidelity of the imprinting process, even in the absence of detailed analysis. However, refractive effects at small q_z are different for the imprint master (silicon) and the imprinted material (polymer) due to their different electron densities, resulting in differences in the two patterns at small q_z. In addition, the dynamic scattering effects give rise to a streak of enhanced scattering along q_r, shown in Figure 2a,b when the outgoing angle (α_f) is equal to the critical angle for the materials.

Although a rigorous analysis of the entire GISAXS pattern is beyond the scope of this paper,[22–24] detailed quantitative morphological information can be obtained from studying the BRs. The position of the BRs along q_r is related to the grating periodicity, while the

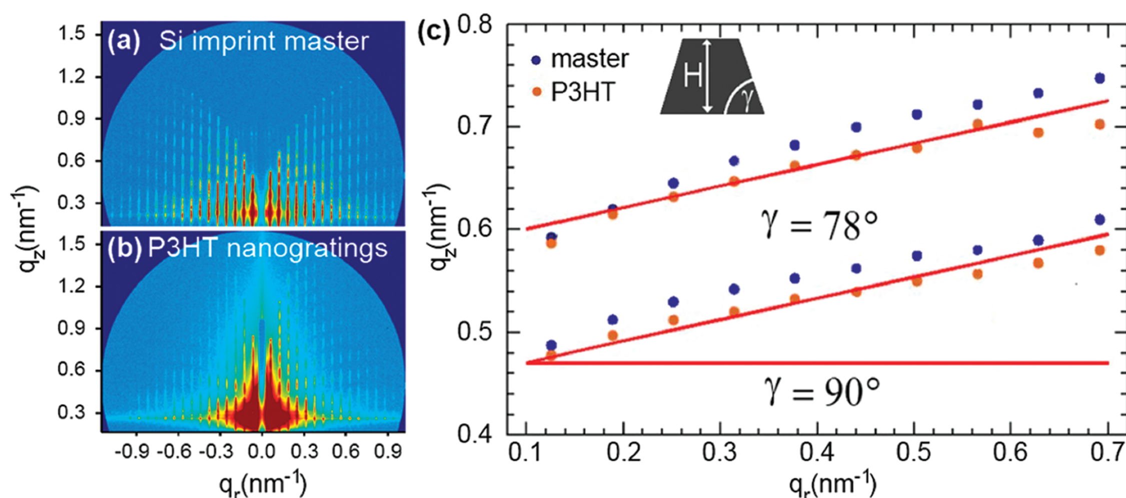

Figure 2. Two-dimensional GISAXS patterns of (a) silicon imprint master and (b) nanoimprinted P3HT. (c) Diffraction peak positions of the second and third BR maxima for the imprint master (blue circles) and P3HT nanogratings (red circles) in the q_r−q_z plane. Solid lines represent the calculated peak positions with the corresponding side-wall angles. Inset: Schematic master trapezoidal cross section.

BR intensity modulation along q_z contains information about the pattern feature height (*H*). For both the silicon master and imprinted P3HT, the spacing between the two adjacent BRs is 0.063 nm^{-1}, corresponding to a 99.7 nm grating periodicity and consistent with the lithographically defined distance of 100 nm. The imprint master feature height of 54.6 nm is obtained from the 0.115 nm^{-1} modulation period along each BR. The imprinted polymer film has a feature height of 52.4 nm, implying that nearly the entire depth of the master was imprinted into the P3HT film. The relative roughness of the top and bottom surfaces is primarily responsible for the damping of the intensity modulation along BRs; we can estimate a relative roughness less than 1.3 nm between top and bottom surfaces, based upon the q_z range over which the intensity falls by 1/*e*. This simple calculation does not include the form factor, and inclusion of this factor only reduces the estimated roughness of 1.3 nm. The GISAXS measurements confirm an excellent fidelity of the imprinting process.

The side-wall slope angle can be directly measured from the phase shift in the BR modulations with q_x.[25] In Figure 2c, the positions of the second and third maxima along the BRs are shown for both the master and the imprinted polymer film. Theoretically, for a side-wall angle (γ), the diffraction maxima of the same order (along the BR) will form a straight line with a slope of ($90°-\gamma$).[25] From the data shown in Figure 2c, we approximate the side-wall angles for both the master and imprinted P3HT (open circles) of 78 ± 1° (solid line). These measurements are consistent with cross-sectional SEM images (Figure 1c).

GIWAXS patterns, acquired simultaneously with the GISAXS measurements, provide detailed information about the polymeric molecular structure, including the lattice constants, coherence lengths, and orientations of the P3HT domains. The radial scattering profiles, extracted from the GIWAXS images, were well-described by Gaussian profile, $\exp(-(q-q_o)^2/2\Delta q^2)$, along with a smoothly varying background. Here the P3HT lattice constant is $a = 2\pi/q_o$ and the coherence length is $\zeta = \pi/(\Delta q)$, a value often associated with the average grain size.[26] We have not included strain-induced broadening in the present analysis.[27] A uniform P3HT thin film, annealed at 150 °C for 5 min, was also investigated as a control. We adopt the standard crystallographic notation for P3HT where the ⟨100⟩ is the layering direction, ⟨010⟩ is the π-stacking direction, and ⟨001⟩ is along the backbone direction.[14,15,17,28] For the P3HT control film, a well-defined (100) P3HT lamellar peak along the q_z direction (Figure 3a) indicates that the lamellar stacking direction is predominately aligned along the surface normal direction. We observe the (010) peak oriented along q_r consistent with the P3HT $\pi-\pi$ stacking direction being parallel to the substrate. The orientation of the (100) and (010) peaks confirm an edge-on chain conformation (Figure 1a) for the control P3HT film, in agreement with previous studies.[14,15,17] The invariance of the scattering patterns with azimuthal sample rotation verified the absence of preferred in-plane orientation. We obtain the layer spacing (1.62 nm) and the $\pi-\pi$ stacking distance (0.38 nm) from the (100) and (010) peak positions, respectively. We also calculate the P3HT coherence lengths, 20 nm for the lamellar and 2 nm for $\pi-\pi$ stacking directions, from the respective radial (100) and (010) scattering profiles. The P3HT control film structural parameters are comparable with previously reported values.[14,16,17,28]

The GIWAXS pattern of a nanoimprinted P3HT film differs significantly from that of the control film. Although we observe scattering peaks at the same radial positions, they no longer exhibit a simple edge-on conformation. Further, the scattering pattern depends on the azimuthal alignment of the imprinted grating pattern with respect to the direction of the incident

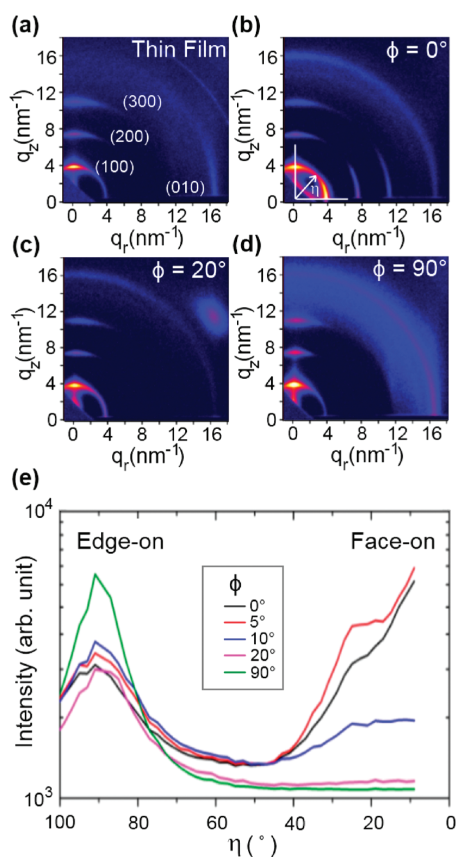

Figure 3. Two-dimensional GIWAXS patterns of (a) uniform P3HT thin film and (b−d) imprinted P3HT taken with azimuthal angle (b) $\phi = 0°$, (c) $\phi = 20°$, and (d) $\phi = 90°$. The azimuthal angle (ϕ) is defined as zero when the grating is parallel to the direction of incident X-rays. (e) Polar angle (η) scans along the (100) peak positions for various ϕ.

X-rays. In Figure 3b−d, GIWAXS scattering patterns are shown for ϕ values ranging from 0 to 90°. At $\phi = 0°$ (Figure 3b), we observe (100), (200), and (300) lamellar scattering peaks along both the q_z and q_r directions, indicating that the imprinting process has realigned some of the lamella parallel to the surface. For the $\phi = 0°$ imprinted film, the (010) reflection exhibits intensity along the q_z axis that is not observed for the control film. Together, these results indicate both edge-on and face-on orientations for the imprinted film. While all polymer domains with edge-on orientations contribute to the (100) peak along q_z, only face-on domains with their backbones aligned with the imprinted grooves satisfy the Bragg condition for the (100) peak along q_r. The absence of a strong (100) peak along q_r for $\phi > 20°$ (shown in Figure 3c,d) demonstrates that the backbones associated with the face-on domains are preferentially aligned along the imprinted grooves. The (010) peak along the q_z direction, arising from π-stacking of the face-on domains, satisfies the Bragg condition regardless of in-plane sample rotation and hence remains visible at all ϕ. The 1D polar scans obtained at (100) peak position from the scattering patterns with different ϕ (Figure 3e) confirm the narrow in-plane orientation distribution of the P3HT backbones with respect to the imprinted grating pattern. In the polar scans, the peak at $\eta = 90$ and 0° corresponds to the edge-on and face-on oriented P3HT domains, respectively (Figure 1a). The intensity of the $\eta = 0°$ peak decreases rapidly with increasing ϕ, and completely disappears at about $\phi = 20°$, indicating that the backbones of the face-on domains are well-aligned along the grating grooves within an angular range of ∼20° full width at half-maximum (fwhm). However, the presence of the (010) peak along q_r for all ϕ suggests that the backbones of the edge-on domains are still randomly oriented in the plane of the substrate. Moreover, the ratio of the integrated intensity between the (010) peak along q_r and (100) peak along q_z remains the same for both $\phi = 0$ and 90°, indicating that the observed (010) scattering is mainly coming from the π-stacking of the edge-on domains. This further implies that little or none of the P3HT backbones are oriented vertically in the nanogratings, in contrast to a previously published study where the vertical rather than face-on orientation was deduced on the basis of the absence of the (010) reflection along the q_z (out-of-plane) direction.[18] Since this reflection is clearly observed in our study, their "missing reflection" might result from the following: (1) the much higher background scattering, (2) poor counting statistics, and (3) the much weaker X-ray source (conventional source compared to the synchrotron-based source used in the present study).

In situ GISAXS measurements of imprinted P3HT films at increasing temperatures show a rapid decay of higher-order BRs, indicating a smoothing-out of the imprinted pattern features (see Supporting Information, S1). However, the first-order BR peak remains at temperatures as high as 200 °C (inset in Figure 4a), showing that remnants of the imprinted profile exist even at this elevated temperature. The extinction of higher-order BRs indicates a transformation from a trapezoidal imprinted profile to a sinusoidal-like height profile, consistent with previous studies of imprinted polystyrene films using critical dimension small-angle X-ray scattering, specular X-ray reflectivity, and optical measurements.[29−32]

Although the imprinted P3HT morphology largely disappears at elevated temperatures, the imprint-induced molecular orientation remains present. The GIWAXS pattern of an imprinted P3HT film at 200 °C at $\phi = 0$ shows evidence of face-on oriented P3HT domains (Figure 4a) (see Supporting Information S1 for other annealing temperatures). The 1D scattering profiles along the q_z and q_r radial directions were extracted from 2D scattering images in the vicinity of the (100) peak and fitted to a Gaussian line shape (discussed above). In the fitting analysis, we have included the effects of refraction, beam divergence, beam bandwidth, and geometric smearing.[26] The fit-determined temperature-dependent lattice constant and coherence length are similar for both the edge-on and

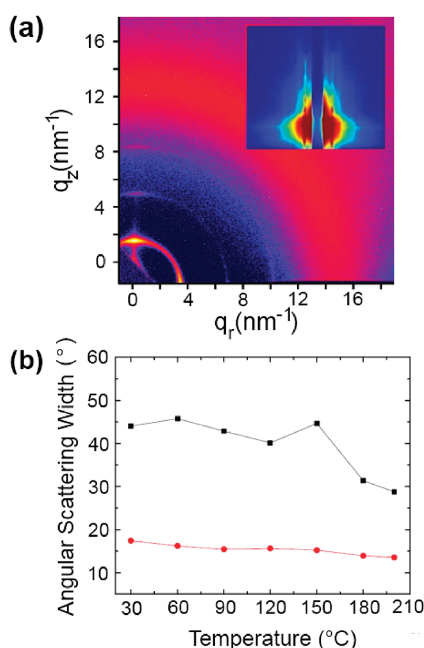

Figure 4. (a) Two-dimensional GIWAXS pattern at 200 °C with corresponding GISAXS pattern (inset). (b) Temperature-dependent angular scattering width for edge-on (red) and face-on (black) oriented P3HT domains obtained from Gaussian fits to the (100) scattering profiles during *in situ* heating.

face-on orientations, whereas the angular scattering width differs significantly for the two orientations. With increasing temperature, the lattice constants for both domain orientations increase monotonically from 1.65 nm at 30 °C to 1.80 nm at 200 °C. Within our resolution, after accounting for refraction effects, there is no significant difference between the lattice constants for the face-on and edge-on configurations. At 30 °C, the coherence lengths for edge-on and face-on oriented P3HT domains, 25 and 30 nm, were similar to those of P3HT control films heated to 150 °C and about a factor of 2 larger than the same films at 30 °C prior to annealing. During a second heating cycle of the imprinted film (the first heating cycle was carried out during the imprinting) the coherence length increased by about ~5 nm for the edge-on oriented domains and ~10 nm for the face-on oriented domains. This increase may be due to the relaxation of temperature-dependent strain effects after removing the master.

The bimodal distribution of the scattering profiles for the ⟨100⟩ peak at $\phi = 0$ (see Figure 3e) provides information on the polar angular widths of the edge-on and face-on orientations. To obtain the profile widths, $\Delta\eta$, we have fit the data in two regions, $70° < \eta < 110°$ for the edge-on orientation and $8° < \eta < 45°$ for the face-on orientation to Gaussian profiles. The data for $\eta < 8°$ was not used due to the strong refraction affects, and the peak position was fixed to $\eta = 0°$ due to the symmetry. At 30 °C for the face-on orientation, $\Delta\eta = 44°$ fwhm (calculated from the Gaussian widths), which is more than twice the 17° fwhm of the edge-on orientation. For comparison, the edge-on domains of the control film exhibit a 13° fwhm. This relatively narrower angular spread of the edge-on domains results from crystal nucleation which occurs at the flat silicon substrate.[14] Similarly, the rough and titled side walls of the imprint master may contribute to the broader angular spread observed for the face-on domains. Upon annealing of the imprinted film—in the absence of the master—$\Delta\eta$ decreases (see Figure 4b) with increasing temperature, suggesting that the vapor interface has a strong effect on the P3HT orientation.

This study provides insight into the structure and morphology of flat and imprinted P3HT thin films. The edge-on configuration observed on flat substrates is likely the lowest energy configuration since it maximizes the coverage of the low-energy methyl groups at both interfaces. This same driving force is believed to be the origin of surface freezing in chain molecules.[33] For the imprinted film, with its considerable side-wall area, the observed ~90° reorientation is likely driven by the reduction of the side-wall interfacial energy, which induces the ⟨100⟩ direction to be along the local surface normal. However, we cannot rule out other factors such as flow-induced reorientation,[10] which may also contribute. Despite the smoothing-out of the topographical profile with increasing temperature, the molecular orientation does not simply restore to the edge-on configuration; rather, both orientations remain. Evidently, annealing (to 200 °C) does not randomize the molecular orientation but instead relaxes imprint-induced strain while simultaneously allowing the imprint-induced orientations to grow and become better defined. This suggests that a wide range of techniques that induce mild orientational bias may be amenable to directing P3HT assembly when coupled with suitable annealing. Finally, the imprint process partially aligns the P3HT chain backbones along the imprinted groove direction. Combined, these results demonstrate that nanoimprint is a powerful tool for controlling molecular orientation in semiconducting polymer materials. The ability to simultaneously control nanometer-scale order and topography, while selecting the desired molecular orientation, should provide new opportunities for an improved understanding of the structure–properties relationship in organic devices since their anisotropic structural and electronic properties are difficult to ascertain in conventional, poorly oriented samples.

METHODS AND MATERIALS

We imprinted (Nanonex NX-B200 instrument) 10 × 10 mm^2 areas of 100 nm thick P3HT films (Rieke Metals, $M_w \approx 50\,000$ g·mol^{-1}, regioregularity ~95%, 2 wt % in chlorobenzene) spin-cast onto silicon substrates using a silicon master imprint template prepared using interference lithography.[34]

The master template pattern consisted of a uniform 100 nm pitch grating with 50 nm deep trapezoidal-shaped grooves. To facilitate release of the master after imprinting, a 1−2 nm thick low-energy coating (perfluorodecyltrichlorosilane) was deposited on the template using a vapor deposition process.

Grazing-incidence small- and wide-angle X-ray scattering (GISAXS and GIWAXS) measurements were performed at the X9 undulator-based beamline at the National Synchrotron Light Source, Brookhaven National Laboratory. The incident X-ray beam (λ = 0.0886 nm) was collimated using slits and focused onto the sample position using Kirkpatrick−Biaz mirrors. This provides a 200 μm wide by 80 μm high spot at the sample position whose footprint along the sample spreads out by the inverse incident angle. The sample stage was located inside the vacuum chamber (pressure ~ 40 Pa) where both the incident angle and azimuthal rotations are computer controlled. A two-dimensional charged-coupled device (CCD) detector was positioned ~270 mm from the center of the sample stage to collect the GIWAXS images inside the same vacuum chamber. The GISAXS images were collected by a second CCD detector located at a distance 3.5 m from the sample. A rectangular beam stop was positioned to block the primary and the reflective beams. Data conversion to q space was accomplished by calibration using Silver Behenate powder.

For a fixed azimuthal angle of the sample, the in-plane component of **q** rotates slightly as q_z is increased. Thus, to obtain a complete Bragg rod around an in-plane position, the scattering intensity was integrated while the samples were rotated azimuthally at a constant angular rate. The extent of q_z was determined by the range of the azimuthal angle ϕ. Increasing the ϕ range also increased the diffuse background.

For thermal annealing experiment, the scattering patterns were obtained every 30 °C and the effective heating rate was 10 °C min^{-1}. At each temperature, the sample was equilibrated for 10 min before collecting the X-ray scattering patterns.

Acknowledgment. This research is supported by the U.S. Department of Energy, Basic Energy Sciences, by the Materials Sciences and Engineering Division (H.H., X.L., and B.O.) and through the Center for Functional Nanomaterials (K.Y. and C.B.), which is supported under Contract No. DE-AC02-98CH10886. This work was partially supported by the Energy Laboratory Research and Development Initiative at Brookhaven National Laboratories. We thank Lin Yang and Danvers Johnston for scientific discussions and technical assistance. We are also indebted to Shalom Wind and John Kymissis for the use of the Columbia University Nanonex Imprinting Tool.

Supporting Information Available: GIWAXS (top) and GISAXS (bottom) patterns of P3HT nanograting at selected temperature during *in situ* thermal annealing. This material is available free of charge *via* the Internet at http://pubs.acs.org.

REFERENCES AND NOTES

1. Mele, E.; Di Benedetto, F.; Persano, L.; Cingolani, R.; Pisignano, D. Multilevel, Room-Temperature Nanoimprint Lithography for Conjugated Polymer-Based Photonics. *Nano Lett.* **2005**, *5*, 1915–1919.
2. Li, H. W.; Huck, W. T. S. Ordered Block-Copolymer Assembly Using Nanoimprint Lithography. *Nano Lett.* **2004**, *4*, 1633–1636.
3. Hu, Z. J.; Baralia, G.; Bayot, V.; Gohy, J. F.; Jonas, A. M. Nanoscale Control of Polymer Crystallization by Nanoimprint Lithography. *Nano Lett.* **2005**, *5*, 1738–1743.
4. He, X.; Gao, F.; Tu, G.; Hasko, D. G.; Hüttner, S.; Greenham, N. C.; Steiner, U.; Friend, R. H.; Huck, W. T. S. Formation of Well-Ordered Heterojunctions in Polymer:PCBM Photovoltaic Devices. *Adv. Funct. Mater.* **2011**, *21*, 139–146.
5. He, X. M.; Gao, F.; Tu, G. L.; Hasko, D.; Huttner, S.; Steiner, U.; Greenham, N. C.; Friend, R. H.; Huck, W. T. S. Formation of Nanopatterned Polymer Blends in Photovoltaic Devices. *Nano Lett.* **2010**, *10*, 1302–1307.
6. Austin, M. D.; Ge, H. X.; Wu, W.; Li, M. T.; Yu, Z. N.; Wasserman, D.; Lyon, S. A.; Chou, S. Y. Fabrication of 5 nm Linewidth and 14 nm Pitch Features by Nanoimprint Lithography. *Appl. Phys. Lett.* **2004**, *84*, 5299–5301.
7. Jung, G. Y.; Johnston-Halperin, E.; Wu, W.; Yu, Z. N.; Wang, S. Y.; Tong, W. M.; Li, Z. Y.; Green, J. E.; Sheriff, B. A.; Boukai, A.; *et al.* Circuit Fabrication at 17 nm Half-Pitch by Nanoimprint Lithography. *Nano Lett.* **2006**, *6*, 351–354.
8. Chou, S. Y.; Krauss, P. R.; Renstrom, P. J. Imprint Lithography with 25-Nanometer Resolution. *Science* **1996**, *272*, 85–87.
9. Zheng, Z. J.; Yim, K. H.; Saifullah, M. S. M.; Welland, M. E.; Friend, R. H.; Kim, J. S.; Huck, W. T. S. Uniaxial Alignment of Liquid-Crystalline Conjugated Polymers by Nanoconfinement. *Nano Lett.* **2007**, *7*, 987–992.
10. Hu, Z. J.; Muls, B.; Gence, L.; Serban, D. A.; Hofkens, J.; Melinte, S.; Nysten, B.; Demoustier-Champagne, S.; Jonas, A. M. High-Throughput Fabrication of Organic Nanowire Devices with Preferential Internal Alignment and Improved Performance. *Nano Lett.* **2007**, *7*, 3639–3644.
11. DeLongchamp, D. M.; Vogel, B. M.; Jung, Y.; Gurau, M. C.; Richter, C. A.; Kirillov, O. A.; Obrzut, J.; Fischer, D. A.; Sambasivan, S.; Richter, L. J.; *et al.* Variations in Semiconducting Polymer Microstructure and Hole Mobility with Spin-Coating Speed. *Chem. Mater.* **2005**, *17*, 5610–5612.
12. Yang, H. H.; LeFevre, S. W.; Ryu, C. Y.; Bao, Z. N. Solubility-Driven Thin Film Structures of Regioregular Poly(3-hexyl thiophene) Using Volatile Solvents. *Appl. Phys. Lett.* **2007**, 90.
13. Sirringhaus, H.; Wilson, R. J.; Friend, R. H.; Inbasekaran, M.; Wu, W.; Woo, E. P.; Grell, M.; Bradley, D. D. C. Mobility Enhancement in Conjugated Polymer Field-Effect Transistors through Chain Alignment in a Liquid-Crystalline Phase. *Appl. Phys. Lett.* **2000**, *77*, 406–408.
14. Kline, R. J.; Mcgehee, M. D.; Toney, M. F. Highly Oriented Crystals at the Buried Interface in Polythiophene Thin-Film Transistors. *Nat. Mater.* **2006**, *5*, 222–228.
15. Yang, H. C.; Shin, T. J.; Yang, L.; Cho, K.; Ryu, C. Y.; Bao, Z. N. Effect of Mesoscale Crystalline Structure on the Field-Effect Mobility of Regioregular Poly(3-hexyl thiophene) in Thin-Film Transistors. *Adv. Funct. Mater.* **2005**, *15*, 671–676.
16. Chang, J. F.; Sun, B. Q.; Breiby, D. W.; Nielsen, M. M.; Solling, T. I.; Giles, M.; McCulloch, I.; Sirringhaus, H. Enhanced Mobility of Poly(3-hexylthiophene) Transistors by Spin-Coating from High-Boiling-Point Solvents. *Chem. Mater.* **2004**, *16*, 4772–4776.
17. Sirringhaus, H.; Brown, P. J.; Friend, R. H.; Nielsen, M. M.; Bechgaard, K.; Langeveld-Voss, B. M. W.; Spiering, A. J. H.; Janssen, R. A. J.; Meijer, E. W.; Herwig, P.; *et al.* Two-Dimensional Charge Transport in Self-Organized, High-Mobility Conjugated Polymers. *Nature* **1999**, *401*, 685–688.
18. Aryal, M.; Trivedi, K.; Hu, W. C. Nano-confinement Induced Chain Alignment in Ordered P3HT Nanostructures Defined by Nanoimprint Lithography. *ACS Nano* **2009**, *3*, 3085–3090.
19. Hofmann, T.; Dobisz, E.; Ocko, B. M. Grazing Incident Small Angle X-ray Scattering: A Metrology To Probe Nanopatterned Surfaces. *J. Vac. Sci. Technol., B* **2009**, *27*, 3238–3243.
20. Scan ranges of ±3° were used to measure P3HT nanogratings, whereas a smaller range of ±1° was used for the strongly scattering silicon stamp in order to avoid saturation of individual detector pixels.
21. Born, M.; Wolf, E. *Principles of Optics; Electromagnetic Theory of Propagation, Interference, and Diffraction of Light*; Pergamon Press: London, 1959; p 803.
22. Lazzari, R. IsGISAXS: A Program for Grazing-Incidence Small-Angle X-ray Scattering Analysis of Supported Islands. *J. Appl. Crystallogr.* **2002**, *35*, 406–421.
23. Rauscher, M.; Salditt, T.; Spohn, H. Small-Angle X-ray Scattering under Grazing Incidence: The Cross Section in the Distorted-Wave Born Approximation. *Phys. Rev. B* **1995**, *52*, 16855–16863.
24. Busch, P.; Rauscher, M.; Smilgies, D. M.; Posselt, D.; Papadakis, C. M. Grazing-Incidence Small-Angle X-ray Scattering from Thin Polymer Films with Lamellar Structures—The Scattering Cross Section in the Distorted-Wave Born Approximation. *J. Appl. Crystallogr.* **2006**, *39*, 433–442.

25. Hu, T. J.; Jones, R. L.; Wu, W. L.; Lin, E. K.; Lin, Q. H.; Keane, D.; Weigand, S.; Quintana, J. Small Angle X-ray Scattering Metrology for Sidewall Angle and Cross Section of Nanometer Scale Line Gratings. *J. Appl. Phys.* **2004**, *96*, 1983–1987.
26. Smilgies, D. M. Scherrer Grain-Size Analysis Adapted to Grazing-Incidence Scattering with Area Detectors. *J. Appl. Crystallogr.* **2009**, *42*, 1030–1034.
27. Baker, J. L.; Jimison, L. H.; Mannsfeld, S.; Volkman, S.; Yin, S.; Subramanian, V.; Salleo, A.; Alivisatos, A. P.; Toney, M. F. Quantification of Thin Film Crystallographic Orientation Using X-ray Diffraction with an Area Detector. *Langmuir* **2010**, *26*, 9146–9151.
28. Kline, R. J.; McGehee, M. D.; Kadnikova, E. N.; Liu, J. S.; Frechet, J. M. J.; Toney, M. F. Dependence of Regioregular Poly(3-hexylthiophene) Film Morphology and Field-Effect Mobility on Molecular Weight. *Macromolecules* **2005**, *38*, 3312–3319.
29. Jones, R. L.; Hu, T. J.; Soles, C. L.; Lin, E. K.; Reano, R. M.; Casa, D. M. Real-Time Shape Evolution of Nanoimprinted Polymer Structures during Thermal Annealing. *Nano Lett.* **2006**, *6*, 1723–1728.
30. Lee, H. J.; Soles, C. L.; Ro, H. W.; Jones, R. L.; Lin, E. K.; Wu, W. L.; Hines, D. R. Nanoimprint Pattern Transfer Quality from Specular X-ray Reflectivity. *Appl. Phys. Lett.* **2005**, 87.
31. Ding, Y. F.; Ro, H. W.; Germer, T. A.; Douglas, J. F.; Okerberg, B. C.; Karim, A.; Soles, C. L. Relaxation Behavior of Polymer Structures Fabricated by Nanoimprint Lithography. *ACS Nano* **2007**, *1*, 84–92.
32. Patrick, H. J.; Germer, T. A.; Ding, Y. F.; Ro, H. W.; Richter, L. J.; Soles, C. L. Scatterometry for *In Situ* Measurement of Pattern Reflow in Nanoimprinted Polymers. *Appl. Phys. Lett.* **2008**, 93.
33. Ocko, B. M.; Wu, X. Z.; Sirota, E. B.; Sinha, S. K.; Gang, O.; Deutsch, M. Surface Freezing in Chain Molecules: Normal Alkanes. *Phys. Rev. E* **1997**, *55*, 3164–3182.
34. Savas, T. A.; Schattenburg, M. L.; Carter, J. M.; Smith, H. I. Large-Area Achromatic Interferometric Lithography for 100 nm Period Gratings and Grids. *J. Vac. Sci. Technol., B* **1996**, *14*, 4167–4170.